Journal Pre-proof

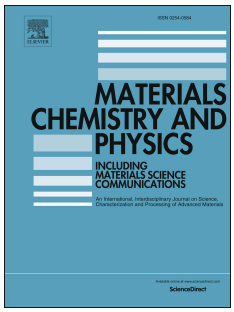

Nanoindentation and structural studies of MgO-doped congruent $LiNbO_3$ single crystals

M.K.Raseel Rahman, B. Riscob, Budhendra Singh, R. Bhatt, Indranil Bhaumik, S. Ganesamoorthy, N. Vijayan, A.K. Karnal, Igor Bdikin, Lekha Nair

PII: S0254-0584(21)00208-X

DOI: https://doi.org/10.1016/j.matchemphys.2021.124425

Reference: MAC 124425

To appear in: *Materials Chemistry and Physics*

Received Date: 29 December 2019

Revised Date: 20 July 2020

Accepted Date: 15 February 2021

Please cite this article as: M.K.R. Rahman, B. Riscob, B. Singh, R. Bhatt, I. Bhaumik, S. Ganesamoorthy, N. Vijayan, A.K. Karnal, I. Bdikin, L. Nair, Nanoindentation and structural studies of MgO-doped congruent $LiNbO_3$ single crystals, *Materials Chemistry and Physics*, https://doi.org/10.1016/j.matchemphys.2021.124425.

Credit author statement

M. K. Raseel Rahman: Conceptualization, Investigation, Writing - Original Draft **B. Riscob:** Methodology, Formal analysis **Budhendra Singh:** Software, Formal analysis **R. Bhatt:** Writing - Review & Editing, Resources **Indranil Bhaumik:** Writing - Review & Editing, Resources **S. Ganesamoorthy:** Project administration **N. Vijayan:** Writing - Review & Editing **A. K. Karnal:** Project administration **Igor Bdikin:** Software, Funding acquisition **Lekha Nair:** Supervision, Writing - Review & Editing, Visualization.

Nanoindentation and structural studies of MgO-doped congruent $LiNbO_3$ single crystals

Nanoindentation and structural studies of MgO-doped congruent $LiNbO_3$ single crystals

M. K. Raseel Rahman[1], B. Riscob[2], Budhendra Singh[3], R. Bhatt[4,6], Indranil Bhaumik[4,6], S. Ganesamoorthy[5,6], N. Vijayan[7], A. K. Karnal[4,5], Igor Bdikin[8], Lekha Nair[1*]

[1] Department of Physics, Jamia Millia Islamia, New Delhi-110025, India.

[2] Institute for Plasma Research, Bhat, Gandhinagar-382428, India.

[3] Department of Physics, Central University of South Bihar, Gaya–824236, India,

[4] Crystal Growth and Instrumentation Section, Laser and Functional Materials Division,

Raja Ramanna Centre for Advanced Technology, Indore-452013, India.

[5] Materials Science Group, IGCAR, Kalpakkam-603102, India.

[6] Homi Bhabha National Institute, Training School Complex, Anushakti Nagar,

Mumbai-400094, India.

[7] CSIR-National Physical Laboratory, In-House BND Group, Dr. K. S. Krishnan Road,

New Delhi–110012, India.

[8] TEMA-NRD, Mechanical Engineering Department and Aveiro Institute of Nanotechnology (AIN), University of Aveiro, 3810–193 Aveiro, Portugal.

*Correspondence e-mail: lnair@jmi.ac.in

Keywords: MgO-doped lithium niobate; Williamson-Hall relation; Raman Analysis; Nanoindentation.

ABSTRACT

The mechanical properties of undoped and 2.0, 4.0 and 6.0 mol% Mg-doped LN single crystals, grown by the Czochralski technique, have been investigated using nanoindentation studies to understand the mechanical deformation behaviour as doping is increased. This has been correlated with structural investigations by powder XRD analysis and Raman spectroscopy. Powder X-ray diffraction measurements show a slight increase in the lattice

parameters as the Mg content is increased in the crystal. The lattice strain developed due to the doping has been calculated by the Williamson-Hall relation. The influence of Mg incorporation on lattice vibrations was analysed using Raman spectroscopy, which indicated no shift in the peak positions with doping, and only slight variation in the intensity and width of the peaks. The grown crystals were subjected to nanoindentation and the Young's modulus and hardness values were obtained by using the Oliver-Pharr method. The results reveal the optimal doping levels of Mg which result in enhanced mechanical strength of lithium niobate single crystals.

1. Introduction

Single crystal lithium niobate ($LiNbO_3$, LN) is a versatile functional material that continues to be under extensive research due to its high demand in areas of device making as diverse as second harmonic generators, electro-optic modulators, optical switches, lasers, holography, photonics and optical communications [1]. It shows excellent nonlinear optical behaviour [2], electro-optic properties [3] and photo refractive effects [4], as well as ferroelectric characteristics [5]. LN single crystals were successfully grown by the Czochralski technique and reported for the first time by Ballman [6].

LN is ferroelectric at room temperature with the R3c space group. Single crystals of LN can be grown from stoichiometric composition (SLN), with the Li/Nb molar ratio of 50:50 as well as from the congruent composition (CLN) with the Li/Nb ratio of 48.6:51.4 [7,8]. It has been well established that many of the physical properties of LN crystals depend on the composition. Stoichiometric LN single crystals, for instance have fewer defects and show large electro-optic coefficient [9] and shorter absorption edge[10]. However, applications of SLN are limited because it shows low laser optical damage resistance and strong light-induced change in the magnitude of the refractive index, as compared to congruent LN crystals [11].

The congruent LN single crystals have good optical quality and compositional uniformity across the length [12], though it is non-stoichiometric, exhibiting specific intrinsic defects like lattice vacancies at Li sites, Nb anti-site defects (Nb_{Li}) and oxygen vacancies in its crystal structure[13,14]. Thus, the congruent composition of LN leads to natural point defects during growth, which generates lattice distortion and geometric strain in the crystalline matrix. Even though innovative approaches have focused on the development of applications with SLN single crystals, CLN single crystals continue to be preferred for applications due to their excellent optical quality. LN crystals are usually grown from the congruent melt using the conventional Czochralski method, since it offers optimal control of parameters during the growth run, ensuring good quality crystals.

For device applications, the LN crystal must be homogeneous in the Li/Nb molar ratio, free from low-angle grain boundaries and cracks, and colourless for optical applications[15]. Optical damage resistance also needs to be improved for LN crystals if they are to function reliably when used for nonlinear optical (NLO) applications. The technologically most efficient method for defeating the optical damage in LN single crystals is doping with optical damage resistant ions. A variety of rare earth ions within a limited threshold concentration can be introduced in the LN lattice as dopants to enhance different functionalities of the crystal. Reports on the undoped and doped CLN crystals suggest that doping with optical damage resistant ions like Mg, In, Zn and Zr etc.[16,17,18,19] may be an efficient way to reduce the optical damage in CLN.

Among these dopants, Mg ion is one of the best materials to enhance optical damage resistance of the LN single crystals. Optical damage resistance by doping with Mg was first reported by Zhong et al. [20]. They observed that LN with a 4.6 or higher mol% of Mg added to the melt can lead to enhanced optical damage resistance to about a hundred times that of the undoped CLN crystal. This was later confirmed by Bryan et al [21]. Doping LN crystals

with Mg reduces point defects [22] and also removes the Nb antisite (Nb_{Li}^{4+}) defects and results in enhanced optical damage resistance. There are several reports available in the literature on Mg:LN crystal growth, phase equilibrium [23,24], defect structure[25,26], properties and characterisation[27,28,29,30].

For device application the grown crystals needs to be sliced and polished with good surface roughness, sometimes even ~1 nm [31]. Hence the utilisation of LN in high-performance devices requires that the grown single crystals have to be subjected to various machining processes including wire saw slicing from an ingot, mechanical polishing or lapping and chemical polishing, to produce a wafer free from cracks and subsurface damage[32,33,34]. In view of this, in the present article the mechanical properties of the grown crystals have been investigated in detail by nanoindentation studies of undoped and 2.0, 4.0 and 6.0 mol% Mg-doped LN single crystals, grown by the Czochralski technique, to understand the change in the mechanical behaviour as Mg doping is increased. Further, the nanoindentation studies have been correlated with structural investigations by powder X-ray analysis and Raman spectroscopy. In addition to this the SHG efficiencies were measured by Kurtz and Perry powder method.

2. Experimental details

2.1. Crystal growth process

For the growth of crystals, MgO (99.999%), Nb_2O_5 (99.999%) and Li_2CO_3 (99.999%) were used as the raw material. 2.0, 4.0 and 6.0 mol% concentrations of Mg were used as the dopant for the current experiments. The Czochralski method using a $MoSi_2$-based resistive furnace, coupled with a Cyberstar automatic diameter controlling crystal puller was used for growing the crystals. The use of a resistive heating furnace with lower thermal gradient in the growth zone- as compared to induction heating furnace- helps to lower the chances of cracking during growth and produces good quality single crystals. During trial experiments, the

thermal gradient in the furnace was optimised by adjusting the crucible position. Platinum crucibles were used for the crystal growth and the temperature of the molten charge was measured by an R-type thermocouple. Eurotherm 902 (single loop) proportional-integral-derivative (PID)-based programmable temperature controller with a resolution of 0.01 K has been used to control the heating and cooling.

The raw materials were mixed properly by ball milling and the starting materials were synthesized by solid-state reaction. Seed crystals used to initiate growth were Z-cut samples of high quality. Rotation rate ~5-25 rotations/minute and pulling rate ~1-3 mm/hour were used to control the growth of the crystal.

2.2. Powder X-ray Diffraction

To confirm the crystal system and for the determination of lattice parameters of undoped and 2, 4 and 6 mol% Mg-doped LN single crystal, fine powders of all the samples were analysed in a Siemens-D500 powder X-ray diffractometer employing CuKα radiation (40 kV, 30 mA). The powder XRD data was recorded in the angular range 15^{o} -140^{o}. The step time and size for the scan were kept at 15 s and 0.02°, respectively.

2.3. Raman Spectroscopy

Raman spectra were measured by using a HORIBA-T64000 Triple Raman Spectrometer equipped with a 514.5 nm Ar^{+} laser made by Spectra Physics, with a beam power of 80 mW as the excitation source. The spectra were recorded for a [001] single-crystal wafer for the 100-1000 cm^{-1} wavenumber range at a temperature of 293 K.

2.4 SHG measurement

The SHG behaviour of the grown crystals were examined by Kurtz and Perry powder technique [35] using potassium dihydrogen phosphate (KDP) as standard reference. A Nd:YAG laser (λ = 1064 nm, input beam energy of 4.7 mJ/pulse, repetition rate of 10 Hz and 8 ns pulse width) was used as a source. The powdered form of crystals of particle size of 125-150 μm, densely filled in a microcapillary of uniform bore and exposed to laser radiation. The SHG signal generated from the micro crystal was collected by a lens and detected by photo multiplier tube.

2.5. Nanoindentation

The elastic properties play a key role in many applications of single crystals. The knowledge of the mechanical deformation behaviour is very important in the making and operation of LN based devices successfully. The mechanical properties such as Young's modulus and hardness etc. of a substance give the information about the strength of the material, which is determined by structural parameters of the crystal such as the atomic arrangement, the interatomic bonding and electronic structure. The nanoindentation testing is a powerful tool based on mechanical response parameters, such as elastic and plastic deformation, dislocation behaviour, residual stresses, fracture, time-dependent behaviour, and stability of crystal surfaces and thin films[36], which are measured under point contact condition. Consequently, nanoindentation techniques have emerged as an important tool to understand and correlate various properties at the molecular level [37]. In this technique, data is recorded as the controlled applied force variation versus the resulting penetration depth of an indenter throughout the entire loading and unloading cycle. By using this technique, one can also calculate hardness, elastic modulus, and stiffness of the sample. However, the obtained parameters are greatly influenced by the surface roughness of the sample.

Mechanical properties of the grown crystals were determined by using a Berkovich pyramidal diamond indenter tip, with a rounding of 20 nm (faces 65.3° from vertical axis), attached to a fully calibrated nanoindenter (TTX-NHT, CSM Instruments) by applying various loads on it. The measurements were done over a range of force from 50-200 mN, with an approach speed of 2000 nm/min. Impressions (distance between two impressions is 50 μm) with varying load were made at different locations on an optically smooth surface of the grown single crystal along the (001) directions. The loading and unloading speed during the measurement was constant, at 20 mN/min with a dwell time of 10 seconds. The formed indentation impressions on the samples were recorded by using an AFM, to see the structural deformations.

3. Results and discussion

3.1. Crystal growth

Fig. 1 a-d shows lapped and polished undoped, 2.0% Mg, 4.0% Mg and 6.0% Mg-doped CLN single crystals, respectively cut along (001) plane (hereafter termed as LN0M, LN2M, LN4M, and LN6M, respectively). For the growth of LN0M, LN2M and LN4M crystals, rotation and pulling rates were 5-25 rotations/minute and 3 mm/hour, respectively, which resulted in crack-free crystals. However, for LN6M crystal, the above mentioned pulling rates resulted in cracked crystals. This is attributed to the lower thermal conductivity in the crystal with higher doping concentration[38]. Hence, pulling rate of 1 mm/hour was employed and a good-quality crack-free LN6M crystal could be grown. More details of the crystal growth have been reported previously in ref. 39. In our earlier study of HRXRD on these Mg:LN single crystal sample it has been reported that the FWHM of the diffraction peak is ~ 29-112 arc sec signifying the good crystalline quality of the grown crystal [39].

Further the Mg content in the wafer is close to that content present in the melt as the segregation coefficient of Mg in LN is close to unity [40]. Also the growth experiment was

carried out in air and chances of loss of MgO due to evaporation is unlikely because of high melting point (~2800°C).

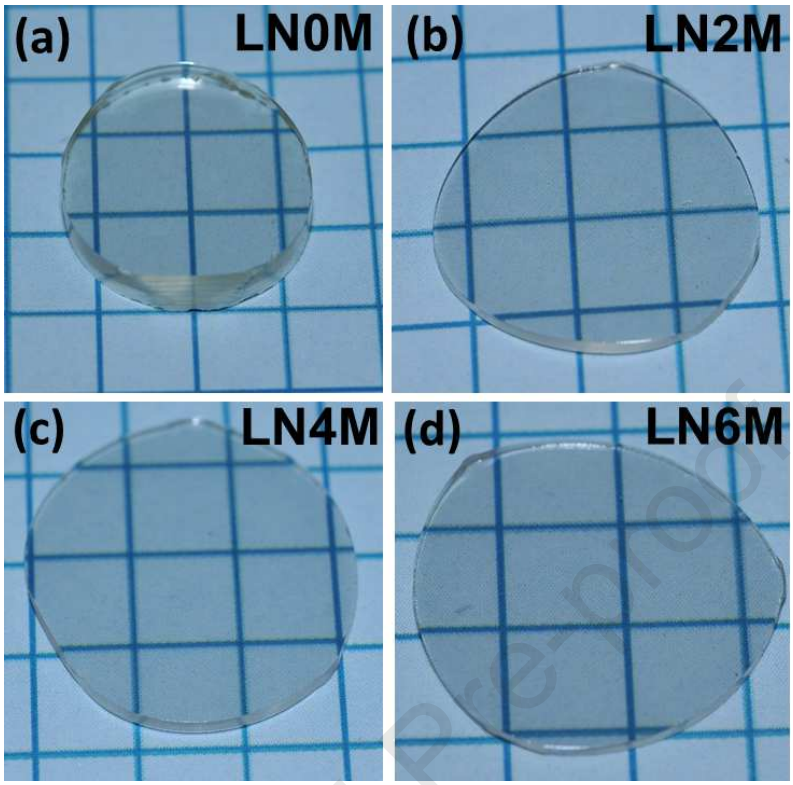

Fig. 1 Lapped and polished (a) LN0M, (b) LN2M, (c) LN4M and (d) LN6M single crystals along the (001) plane.

3.2. Powder X-ray diffraction analysis

To evaluate the effect of Mg addition on the crystal structure of LN, fine powder of the grown crystals was analysed by powder X-ray diffraction(PXRD). The recorded PXRD patterns for LN0M, LN2M, LN4M and LN6M crystals were subjected to Rietveld analysis using Fullprof software to determine the details of the crystal structure. Fig. 2 a-d shows the experimental, calculated, residual and the Bragg peaks for the LN0M, LN2M, LN4M and LN6M crystals respectively. The refined lattice parameters are tabulated as Table 1 along with those calculated for pure CLN by Abrahams & Marsh [41]. The obtained values of the lattice parameter of LN0M is consistent with earlier reports [42]. The refinement software

confirmed that the grown CLN crystals were of a single phase and crystallize in the trigonal (rhombohedral) crystal system with space group R3c. XRD peaks show that there is no significant change in the parent LN lattice due to doping. However, very small variations in the intensity may be due to the particle size and batch preparation.

From Table 1, a small deviation in the lattice parameters was observed with the incorporation of Mg into the LN lattice. A systematic increase in the lattice parameters and the unit cell volume was noted as shown in Fig. 3. These observations are in good agreement with reported results [43,44]. Initially the Mg dopant replaces the Nb_{Li}, further addition of Mg results in incorporation into the Li sites up to a doping concentration of 5.15 mol% [45], which compensates for the Li vacancies. At higher Mg content it replaces both the Li and Nb sites in such a way as to keep Li/Nb ratio within the solubility limit. The Li vacancies initially decrease due to replacement of Nb_{Li} and then increase till 5.15 mol % Mg. Accordingly, the Li/Nb ratio initially remain constant up to 3 mol.% and beyond this it decreases further. As the ionic radius of Mg (86 pm) is higher than Nb (78 pm), but lower than Li (90 pm), a slight increase in the lattice parameter is expected due to incorporation of Mg and the corresponding Li vacancies in the lattice.

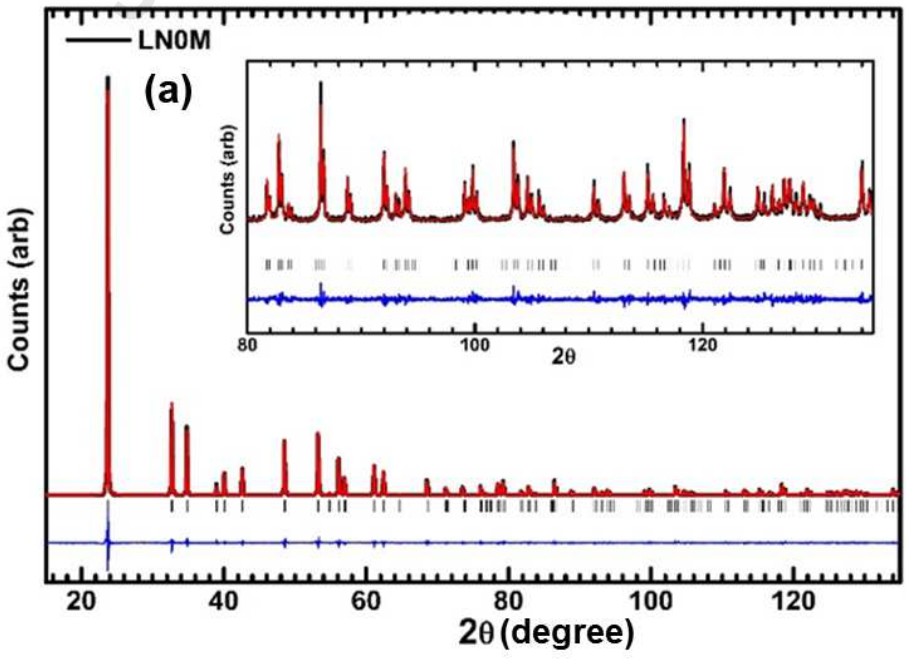

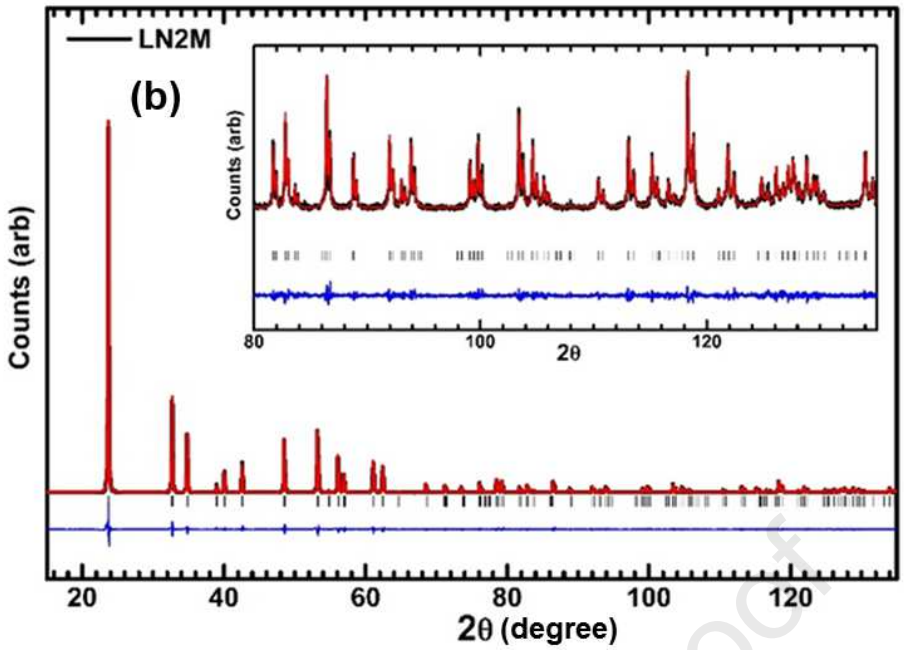

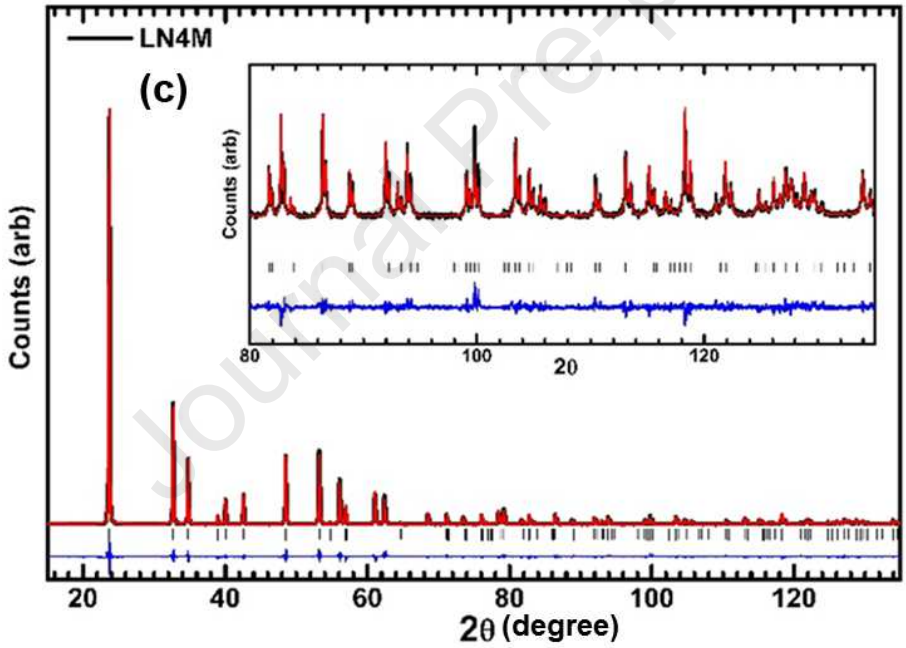

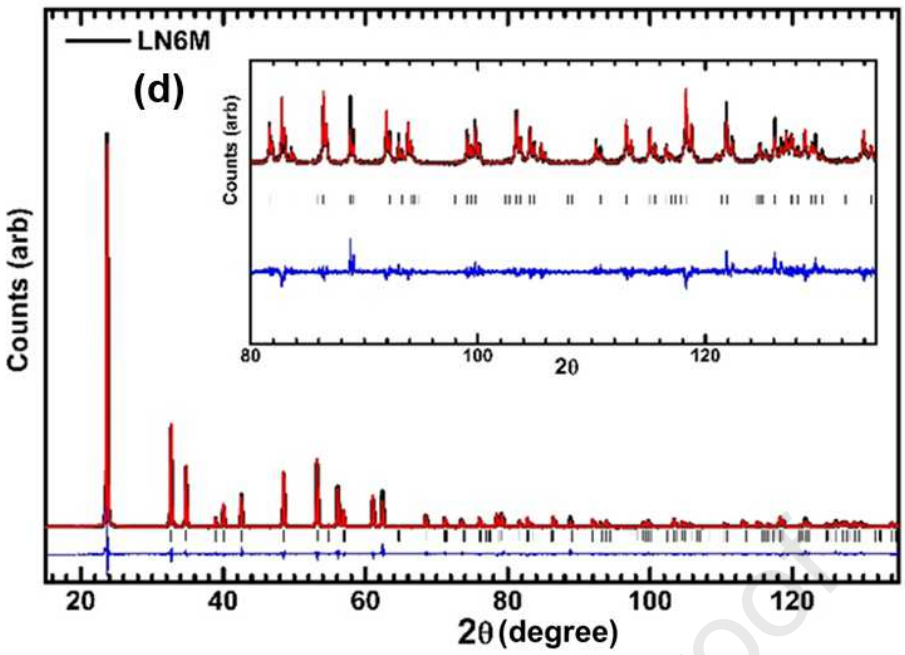

Fig. 2 Rietveld refinement of (a) LN0M, (b) LN2M, (c) LN4M and (d) LN6M crystals, respectively.

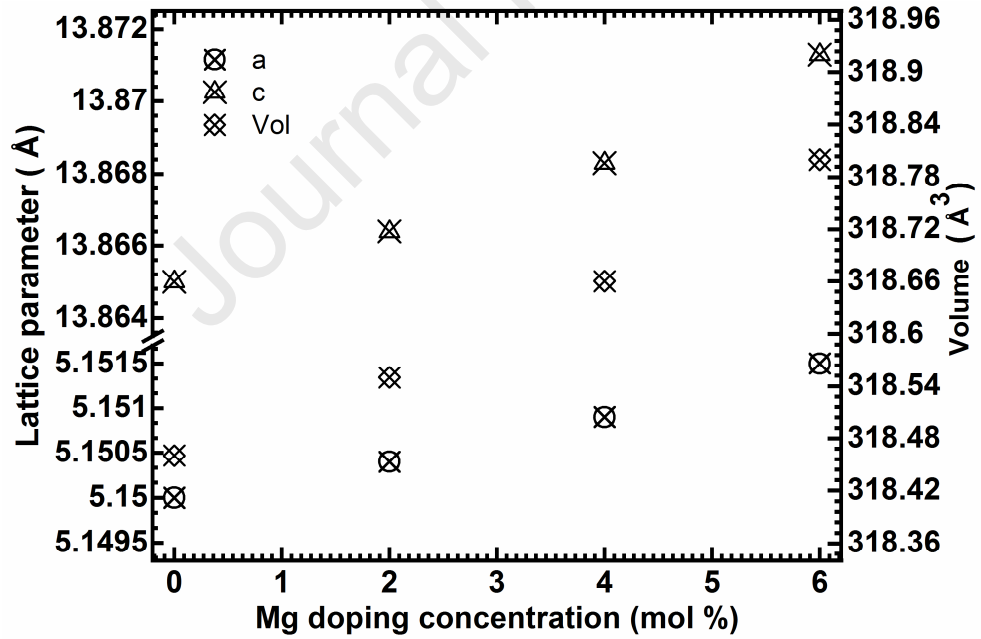

Fig. 3 Variation of lattice parameters and volume with varying Mg concentration.

Table 1. Obtained lattice parameters after Rietveld refinement of LN0M, LN2M, LN4M and LN6M crystals

Crystal Composition	a (**Å**)	c (**Å**)	Volume (**Å^3**)
LN0M	5.1500(3)	13.8650(9)	318.46(9)
LN2M	5.1504(6)	13.8664(8)	318.55(8)
LN4M	5.1509(9)	13.8683(2)	318.66(5)
LN6M	5.1515(4)	13.8713(7)	318.80(4)
Undoped LN†	5.1505(2)	13.8649(6)	318.51(3)

(† calculated by Abrahams &Marsh) [14]

The sources of lattice strain in the crystal lattice can be dislocations, grain boundaries, stacking faults, contact stresses and others[46]. The strain (η) developed in the crystalline lattice is given by the Williamson–Hall relation[47] as follows.

$$\beta cos\theta = \frac{\kappa\lambda}{\tau} + \eta sin\theta \quad (1)$$

where β is the FWHM (full width at half-maximum) in radians, κ is the Scherrer constant, λ is the wavelength of the X-rays, θ is the Bragg diffraction angle of the peak, and τ is the crystallite size. The slope of the $\beta cos\theta$ versus $sin\theta$ plot gives the value of η . In the present study, the value η for LN0M, LN2M, LN4M and LN6M crystals are found to be -1.24 x 10^{-3}, -4.37 x 10^{-4}, -9.01 x 10^{-4} and -4.94 x 10^{-4}, respectively as shown in Fig. 4(a-d). In spite of taking sufficient care for preparation of the sample and evaluation of FWHM and the accuracy of the fitting is not very good. However the negative value of the slope is quite

evident from the plot. Generally, a negative value of η confirms the expansion of the lattice around the substituent Mg ion, as discussed in the earlier section, which leads to strain in the crystal. Compared to undoped LN, the decrease of strain in Mg:LN crystals may be due to the dopant Mg ions well occupied in the crystal lattice. It is interesting to see that the strain for LN6M is less than LN4M and LN2M. As mentioned in the growth condition earlier, the cracks were present in LN6M grown at a pulling and rotation rate of 3 mm h^{-1}, 5-25 r min^{-1} respectively. Hence, we chose at cooling rate of 50 K h^{-1} and a low pulling rate of 1 mm h^{-1} for LN6M. From the low strain value of LN6M, it is clear that the pulling rate during growth has a significant effect on crystalline perfection. The low strain value indicates that the grown Mg:LN crystals are free from strains.

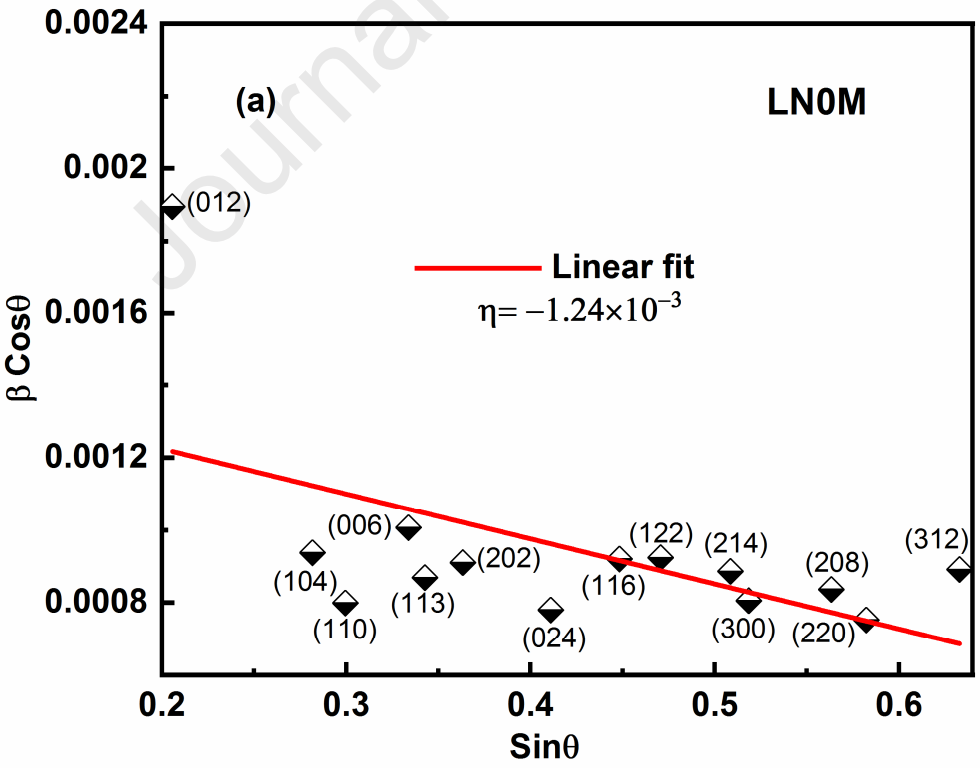

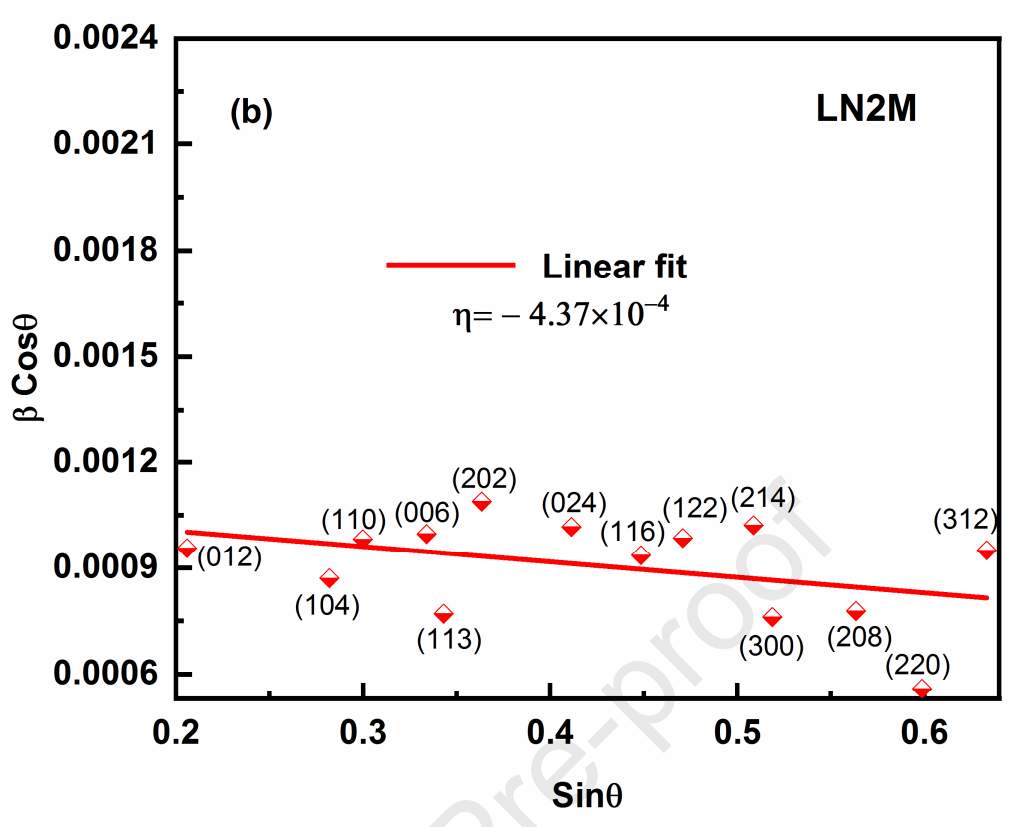

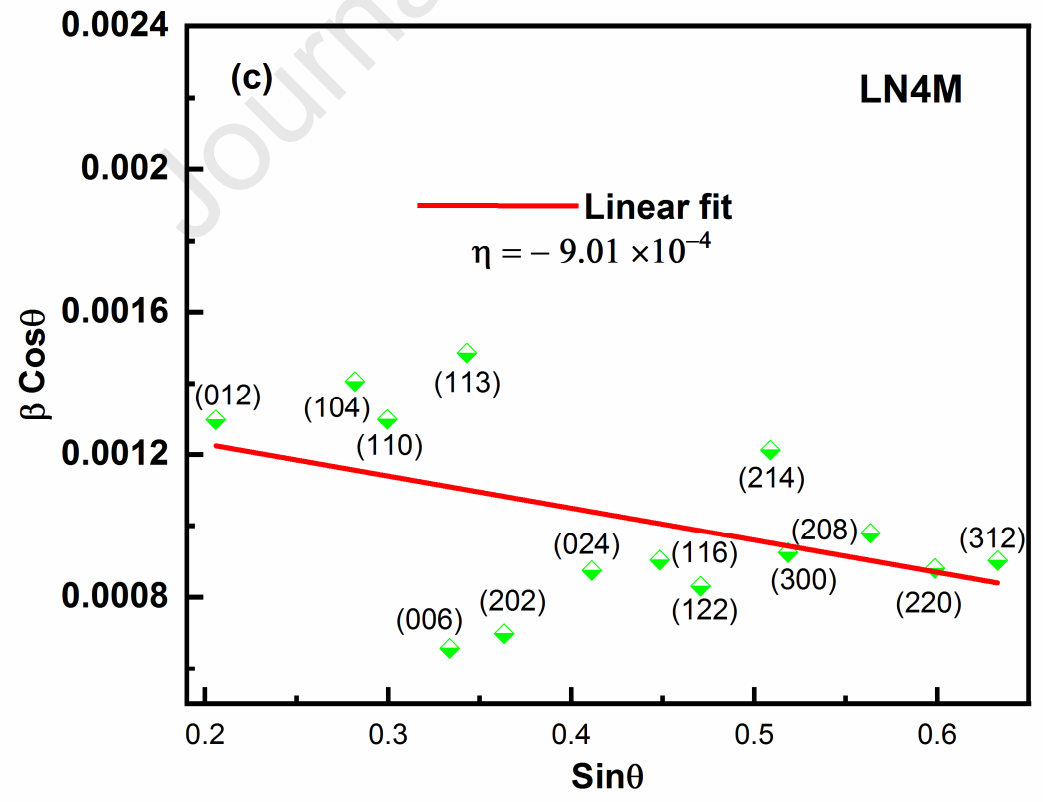

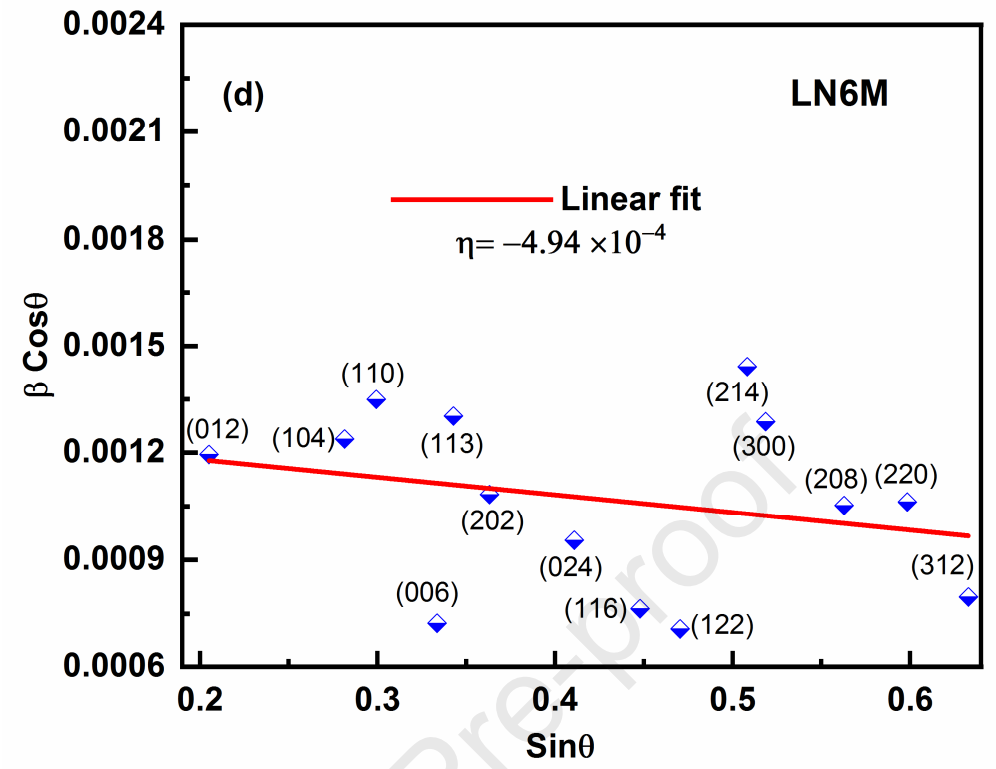

Fig. 4 Williamson–Hall plot for (a) LN0M, (b) LN2M, (c) LN4M and (d) LN6M crystals for calculating strain in the grown crystals

3.3. Raman Analysis

The parameters of Raman spectra are very sensitive to the component of crystal structure, defects, and deviations from the stoichiometry of LN crystal[48]. Fig. 5 shows the Raman spectra of LN0M, LN2M, LN4M and LN6M single crystals which are carried out in the Z(YX)Z scattering direction. The peaks in the spectra of the crystal correspond to various vibrational modes. The spectra indicate that all the doped crystals exhibit the same peak positions as the fundamental phonon modes of undoped LN. The observed peak at 152 and 872 cm^{-1} are due to the E(TO1) and E(LO9) modes of Nb-O vibrations. The E(TO6) mode at about 365cm^{-1} is attributed to Li-O vibration. The E(TO8) mode at about 580cm^{-1} are identified as the stretching vibration of the oxygen octahedron. The E(TO7) band at 432cm^{-1} corresponds to Li-O vibrations[49,50]. There were no variations in the wave numbers of the Raman peaks with Mg

doping concentration, but changes in the Raman intensities and FWHM of the peaks were observed. These observations suggest that the addition of Mg dopant causes no basic structural change in the crystal lattice except for the changes in the concentrations of point defects as analysed by powder XRD. The peak at 872 cm^{-1} is attributed to LO modes of the Li sub-lattice and line-width of the same is correlated to the Li content in the lattice. The line width (FWHM) of the 872 cm^{-1} peak was evaluated by Lorentz fit and its values are 28.46, 32.77, 38.82 and 42.67 cm^{-1} respectively for LN0M, LN2M, LN4M and LN6M sample. The change in half width of the peaks with the addition of Mg indicates the increase in disorder within the crystal structure[51]. The change in FWHM for E(TO1), E(TO7) may be due to the addition of Mg ions which contributes to the disorder in Nb sub-lattice and Li sub-lattice respectively. It is known that Mg ions replace the Nb cations at Li sites first, and further increase of Mg gradually replaces Li from its sites, leaving some Li vacancies. The observed increase in the Raman line-width may be attributed to the presence of vacancies, lattice strain, decrease in Li/Nb ratio and the disorder depending on the the Mg content in the lattice[52]. The presence of Li vacancy defects is in correlation with strain calculation from PXRD data.

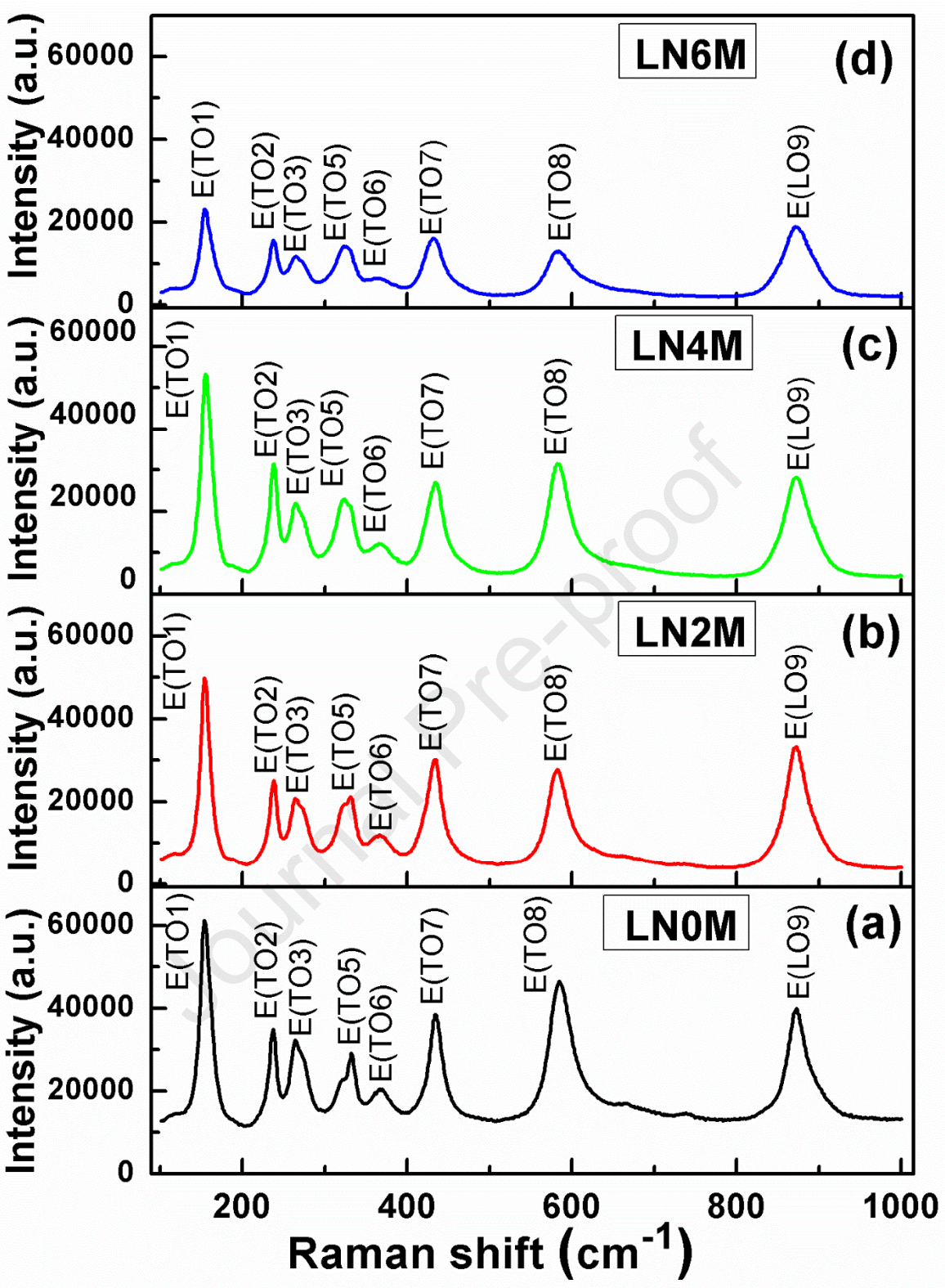

Fig. 5 Raman spectra of (a) LN0M, (b) LN2M, (c) LN4M and (d) LN6M single crystals

3.4 SHG Analysis

The SHG property of undoped and Mg doped LN samples were confirmed by green light (λ= 532 nm) output during SHG measurement as described by section 2.4. Output power values of LN0M, LN2M, LN4M, LN6M samples are given in Table 2. The Mg dopant enhances the NLO efficiency. These observations show that the LN4M samples have high NLO efficiency. The relative SHG efficiency of LN0M, LN2M, LN4M, LN6M are 2.88, 3.11, 3.29 and 3.05 respectively to that of standard KDP crystal.

Table. 2. Relative SHG output

Sample	**Power output**
KDP	13.6 mV
LN0M	39.2 mV
LN2M	42.4 mV
LN4M	44.8 mV
LN6M	41.6 mV

3.5. Nanoindentation

For the present study, well lapped and polished crystals for LN0M, LN2M, LN4M, and LN6M were selected. For this, the crystals were cut along (001) plane and optically polished using fine grade alumina powder. In general the imprint of the indentor may show a slight azimuthal angular dependence due to the anisotropic properties of the crystals, hence the measurements should be done along a particular direction for proper comparison among the samples. If grown along the c axis, LN crystal exhibits characteristic 3 fold symmetric growth ridges in the body part as can be seen as three protruded parts along the edges of the wafers [Fig. 1]. Along these ridges the atomic arrangement is same. Hence to ensure the accuracy in

the measurement, in the present investigation, we have performed the measurements along one of the growth ridges to keep the azimuth orientation of the sample same and to have accuracy in the measured value. In addition, for evaluating the roughness of the surface for proper indentation, the surface topography AFM image was taken. Fig. 6 (a-d) shows low resolution and Fig. 6 (e-h) shows the high-resolution surface topography AFM image for LN0M, LN2M, LN4M and LN6M crystal. The RMS roughness of the polished surface was calculated in a wide area (45 x 45 µm) as well as from the high-resolution AFM image of the small area (25 x 25 µm). The RMS roughness values of the z-cut, well lapped and polished surface are shown in the respective Fig. 6 (a-h).

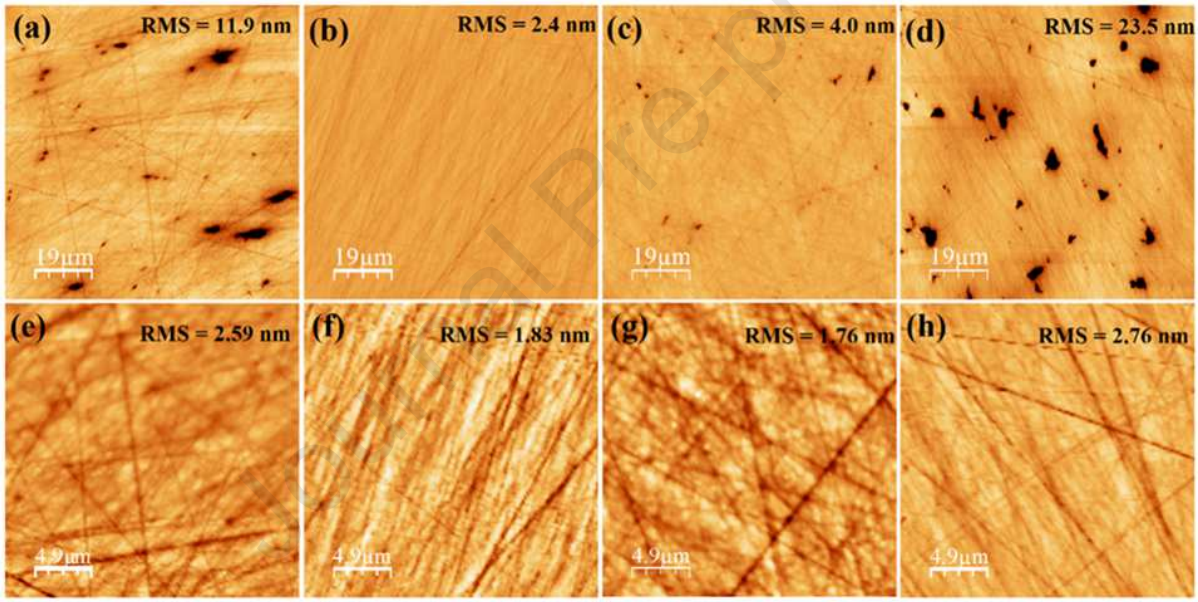

Fig. 6 (a-d) Wide area and (e-h) small area surface topography AFM image for LN0M, LN2M, LN4M and LN6M crystals

The standard Oliver and Pharr method [53] was used to analyse the obtained results. The hardness, H, is determined from the ratio of the peak indentation load to the projected area of the indentation, A_c , i.e.:

$$H = \frac{P_{max}}{A_c} \tag{2}$$

The load independent hardness(H_0) calculated using the relation [53]:

$$H_0 = ka_2 \tag{3}$$

where k is a constant which depends on the geometry of the indenter, $k = 1/24.5$ for Berkovich indenter and a_2 is a constant derived from the polynomial fitting of peak load-indenter displacement plot. The area function A_c was calibrated for a standard silica sample of known hardness with polynomial function [53]:

$$A_c = 24.5h_c^2 + C_1h_c + C_2h_c^{1/2} + C_3h_c^{1/4} + C_4h_c^{1/8} \tag{4}$$

where, h_c is the contact depth, C_1, C_2, C_3 andC_4 are constants.

The stiffness $S\left(\frac{dP}{dh}\right)$ defined as the slope of the unloading segment of the experimental load-displacement curve at the peak load can be expressed as [53]:

$$h_c = h_{max} - 0.75 \times \frac{P_{max}}{S} \tag{5}$$

where h_{max} is the maximum displacement at the peak load, and the second term is the displacement of the specimen surface at the perimeter of the contact at peak load.

Further, the unloading portion of the load-displacement curve is related by the following relation [54]

$$P = \alpha\ (h - h_f)^m \tag{6}$$

where P is the load applied m and α are material constants, h is the indenter displacement, and h_f is the final displacement after complete unloading. After obtaining the parameters, m, by nonlinear curve fitting, the value of, S , can be calculated by differentiating P at the maximum depth of penetration [55],

$$S = \left(\frac{dP}{dh}\right) = \propto m(h_{max} - h_f)^{m-1} \tag{7}$$

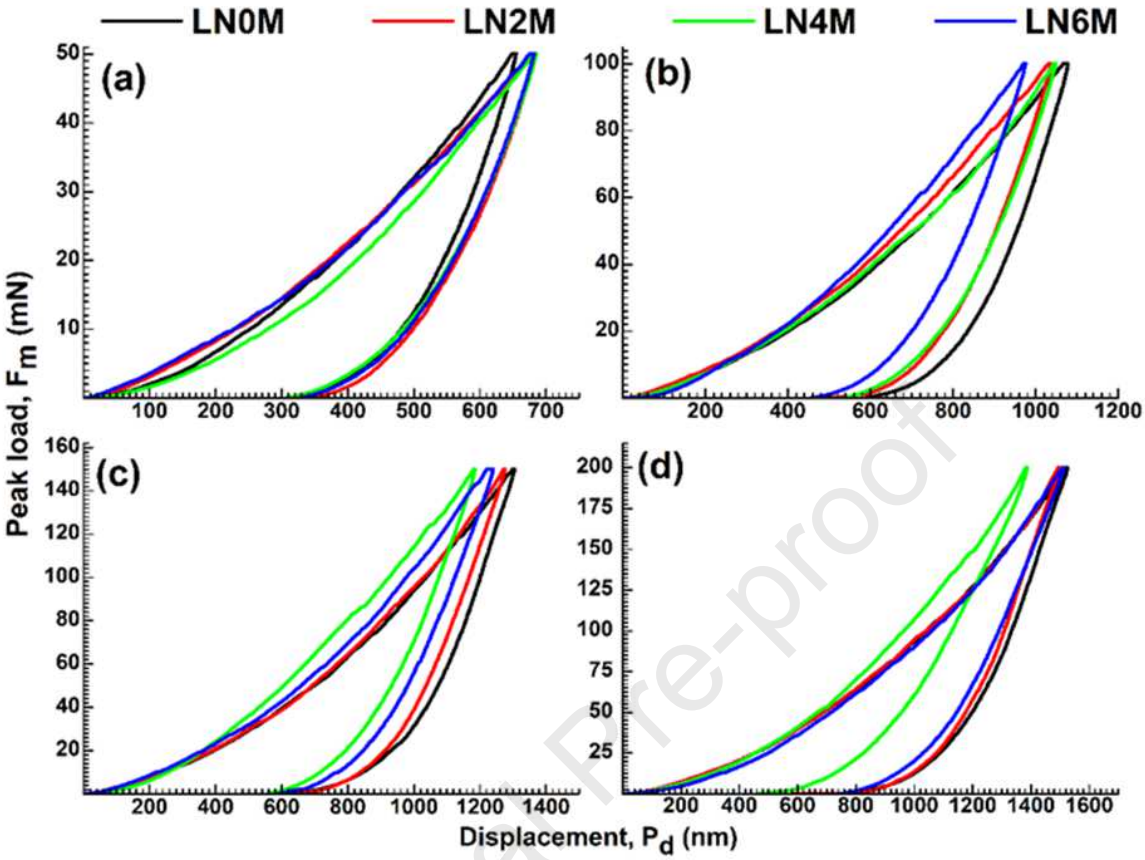

Fig. 7 Typical load-displacement curve on (001) plane of LN0M, LN2M, LN4M and LN6M crystal for (a) 50 mN (b) 100 mN, (c) 150 mN and (d) 200 mN load.

The load -displacement curves (P-h) of undoped as well as all the Mg doped LN crystals show the similar elastic behaviour under the applied force (Fig. 7 a-d). On a closer look, it was observed that the indenter forms only very slight pop-ins. The presence of these pop-in is due to the breaking of the molecular interlayer resulting in a sudden penetration of the indenter into the sample[56]. Further, the existence of these pop-ins is also related to the transition from elastic to plastic regime, which is indicated by the nucleation of plastic deformation due to dislocations, cracks and slips [37]. These observations are in consistence with previous reports on nanoindentation of LN [57,58]. At a particular load, LN2M, LN4M,

and LN6M show comparatively less displacement than LN0M which is evident for the Mg doping gives more rigidity in the crystal structure. The Fig. 8 shows the AFM image of a typical imprint made after nanoindentation, which allows precise topography imaging in a controlled manner. The deformation beneath the indentation area was analysed. No indentation-induced cracking was found in the vicinity of the indentation.

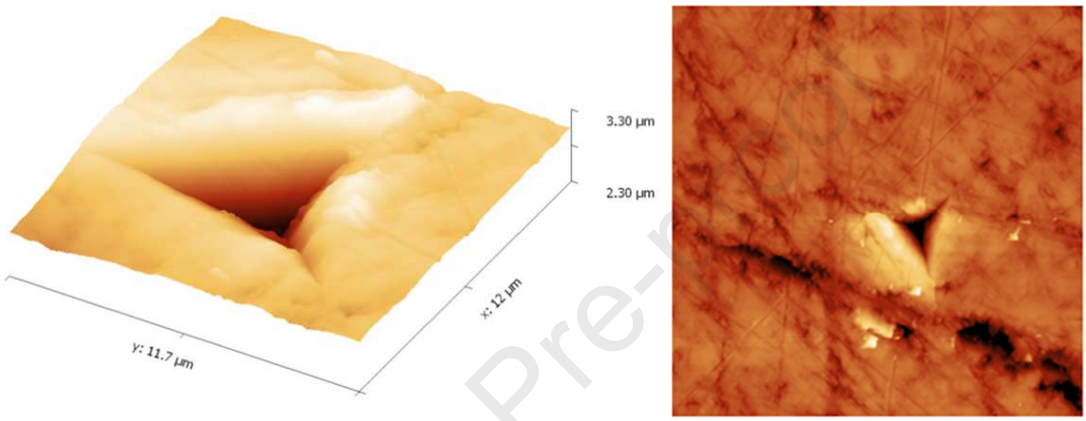

Fig. 8 A topographic image (AFM) of the triangular indentation mark made using Berkovich nano-indenter

Apart from this Young's modulus, hardness and stiffness, were also estimated. The relation between the contact depth and peak load can be formulated as follows[37]:

$$P = a_0 + a_1 h_c + a_2 h_c^2 \tag{8}$$

where P is the peak load, a_0, a_1, a_2 are the constants and h_c is contact depth. Fig. 9 shows the variation of contact depth (h_c) with peak load, for indentation made on the (001) plane of LN0M, LN2M, LN4M and LN6M. The curve was fitted with a polynomial function and the fitted values for a_0, a_1, $a_2$and the load independent hardness (H_0) value calculated from the equation (3) is shown in Table 2. The value of hardness for LN0M, LN2M, LN4M and LN6M are 3.996 GPa, 3.959 GPa, 4.449 GPa, 4.245 GPa respectively. The increase in the

hardness shows that the addition of Mg ions makes the crystal structure of LN mechanically strong. Also, the highest load independent hardness of LN4M crystal suggest that the LN4M crystals are mechanically more stable than others. It is interesting to note that Mg doping concentration of 4-5 mol% is the optimum (threshold) concentration for enhancement of the mechanical properties of LN. This is consistent with the findings of Zhong et al. [20], who have reported that Mg doping concentration of 4-5 mol% resulted in the highest laser damage threshold of Mg:LN crystals due to the decrease in intrinsic defects.

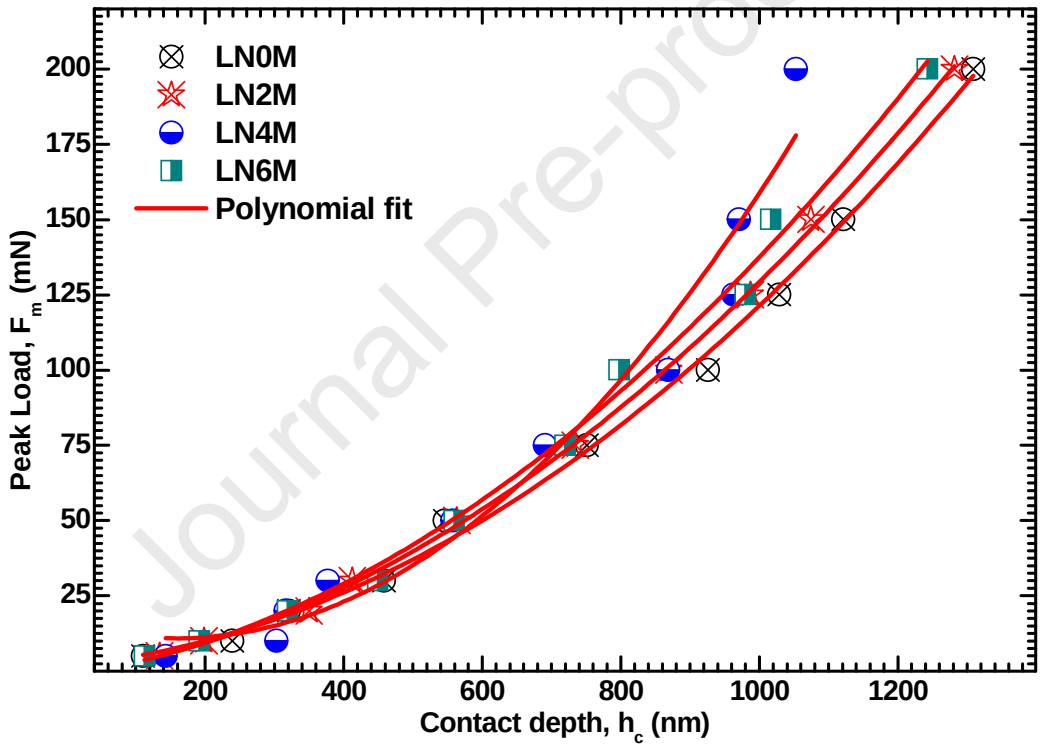

Fig. 9 Variation of contact depth with peak load.

Table 3 The obtained values for the constants a_0, a_1, a_2 and the calculated load independent hardness value of LN0M, LN2M, LN4M, LN6M crystals.

	LN0M	**LN2M**	**LN4M**	**LN6M**
$\mathbf{R^2}$	0.99623	0.99919	0.95389	0.99248
$\boldsymbol{a_0}$	1.78845	-1.21712	16.17387	-1.62725
$\boldsymbol{a_1}$	0.02164	0.03349	-0.06645	0.03527
$\boldsymbol{a_2}$ ***(mN nm^{-2})***	0.0000979	0.0000970	0.000109	0.000104
$\mathbf{H_o}$ **(GPa)**	3.996	3.959	4.449	4.245

Further, the stiffness (S) of the sample vs the contact depth at peak load is shown in Fig. 10. The relation between stiffness and contact depth is given by

$$S = a + bh_c \tag{9}$$

where a is a constant related to indentation tip rounding and the slope b is related to the reduced Young's modulus as[59]

$$\text{Slope} = \frac{2}{\pi} E_r \sqrt{24.5} \tag{10}$$

A linear relationship between the contact depth and initial stiffness was observed. Using linear fitting the value of slope was calculated and substituted in equation 10 in order to calculate the reduced Young's modulus (E_r). The E_r for LN0M, LN2M, LN4M and LN6M were found to be 143.75 GPa, 143.44 GPa, 129.79 GPa and 125.35 GPa respectively. A decrease in the value of Young's modulus was observed with increasing doping concentration of Mg. The obtained hardness and Young's modulus are in agreement with the trend observed by Palatnikov et al. [60].

The result is in agreement with the structural investigation by XRD in which the strain in the lattice is minimum for the doping concentration of 4 mol% of Mg. Also the powder SHG data as described in the previous section shows that SHG performance is best for 4 mol% of Mg doping.

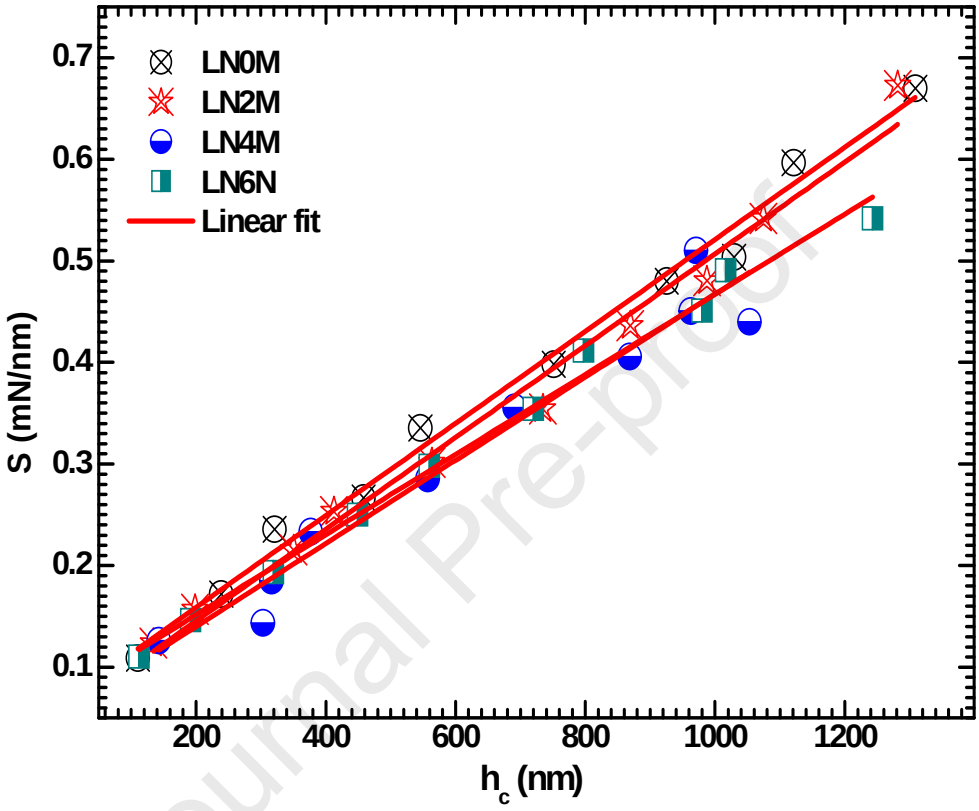

Fig. 10 Variation of initial loading stiffness with the contact depth at peak load

Table 4 Various parameters obtained from the stiffness vs contact depth plot for LN0M, LN2M, LN4M, LN6M crystals

	LN0M	**LN2M**	**LN4M**	**LN6M**
R^2	0.990298	0.98588	0.949241	0.991578
Intercept	0.068075	0.055098	0.05817	0.072583
Slope (mN nm^{-2})	4.53E-04	4.52E-04	4.09E-04	3.95E-04
Slope (GPa)	453	452	409	395
E_r (GPa)	143.75	143.44	129.79	125.35

4. Conclusions

The focus of this study was the investigation of the nanoscale mechanical behaviour of Mg doped LN crystals. Nano-indentation study reveals that the addition of Mg gives high rigidity and mechanical strength to the crystal. The highest load independent hardness is observed for 4 mol% Mg doped LN crystal (LN4M) indicating it as a threshold concentration for the enhancement of mechanical properties, in congruence with the optical damage threshold which has been reported as the highest for the 4 mol% Mg doped LN crystal. Undoped and Mg doped LN single crystals were successfully grown under optimized conditions by using Czochralski technique and variations in crystal structure and NLO behaviour were confirmed using PXRD, Raman and SHG. Powder X-ray diffraction confirms good crystallinity and shows that there no significant change in the parent LN lattice due to Mg doping. A slight increase in the lattice parameters confirms the incorporation of dopant into the LN lattice, and the presence of tensile strain due to vacancies in the crystal structure. The Raman spectra shown no change in vibrational modes of the lattice except a slight variation in the intensity and peak width with addition of Mg. These observations suggest that the addition of Mg makes no basic structural change in the crystal lattice except the change in the concentration

of point defects as analysed from powder XRD. A slight increase in half-width of the peaks with the addition of Mg indicates the increase in disorder within the crystal structure. The Mg dopant enhances the NLO efficiency, and LN4M crystals shows high SHG values.

Acknowledgement

Author M. K Raseel Rahman wishes to acknowledge the University Grants Commission for UGC-Non NET fellowship. Author Budhendra Singh and Igor Bdikin wish to acknowledge the Portuguese Foundation for Science and Technology (FCT) for the financial support: IF/00582/2015, BI (DOUTOR)/6323/2018), UID/EMS/00481/2013-FCT, CENTRO-01-0145-FDER-022083 and Pest-C/EME/UI0481/201.

References

[1] C. Chen, L. Pang, Q. Lu, L. Wang, Y. Tan, Z. Wang, F. Chen, Refractive index engineering through swift heavy ion irradiation of $LiNbO_3$ crystal towards improved light guidance, Scientific reports, 7 (2017) 10805.

[2] M. Imlau, H. Badorreck, C. Merschjann, Optical nonlinearities of small polarons in lithium niobate, Applied Physics Reviews. 2 (2015) 040606.

[3] L. Arizmendi, Photonic applications of lithium niobate crystals, Physica status solidi (a). 201 (2004) 253-283.

[4] K. Buse, Light-induced charge transport processes in photorefractive crystals II: Materials, Applied Physics B. 64 (1997) 391-407.

[5] I. Bhaumik, S. Ganesamoorthy, R. Bhatt, A. K. Karnal, V. K. Wadhawan, P. K. Gupta, K. Kitamura, S. Takekawa, M. Nakamura, The ferroelectric phase transition in lithium tantalate single crystals: A composition-dependence study, Journal of Applied Physics. 103 (2008) 014108.

[6] A.A. Ballman, Growth of piezoelectric and ferroelectric materials by the Czochralski technique, Journal of the American Ceramic Society. 48 (1965) 112-113.

[7] R. Bhatt, I. Bhaumik, S. Ganesamoorthy, B. Riscob, M. Soharab, A. K. Karnal, P. K. Gupta, Control of intrinsic defects in lithium niobate single crystal for optoelectronic applications, Crystals. 7 (2017) 1-23.

[8] B. Riscob, I. Bhaumik, S. Ganesamoorthy, R. Bhatt, N. Vijayan, K. Zimik, A.K. Karnal, G. Bhagavannarayana, P. K. Gupta, Crystal growth of Ru-doped congruent $LiNbO_3$ and investigation of crystalline perfection and optical properties, Journal of Applied Crystallography. 48 (2015) 1753-1760.

[9] F. Abdi, M. Aillerie, P. Bourson, M. D. Fontana, K. Polgar, Electro-optic properties in pure $LiNbO_3$ crystals from the congruent to the stoichiometric composition, Journal of applied physics. 84 (1998) 2251-2254.

[10] R. Bhatt, I. Bhaumik, S. Ganesamoorthy, A. K. Karnal, M. K. Swami, H. S. Patel, P. K. Gupta, Urbach tail and bandgap analysis in near stoichiometric $LiNbO_3$ crystals, Physica status solidi (A). 209 (2012), 176-180.

[11] K. Niwa, Y. Furukawa, S. Takekawa, K. Kitamura, Growth and characterization of MgO doped near stoichiometric $LiNbO_3$ crystals as a new nonlinear optical material, Journal of crystal growth. 208 (2000) 493-500.

[12] Y. L. Chen, J. P. Wen, Y. F. Kong, S. L. Chen, W. L. Zhang, J. J. Xu, G. Y. Zhang, Effect of Li diffusion on the composition of $LiNbO_3$ at high temperature, Journal of crystal growth. 242 (2002) 400-404.

[13] P. Lerner, C. Legras, J. P. Dumas, Stoechiométrie des monocristaux de métaniobate de lithium, Journal of Crystal Growth. 3 (1968) 231-235.

[14] S. C. Abrahams, P. Marsh, Defect structure dependence on composition in lithium niobate, Acta Crystallographica Section B: Structural Science. 42 (1986) 61-68.

[15] J. Trauth, B. C. Grabmaier, The shape of the crystal/melt interface during the growth of lithium niobate crystals by the Czochralski technique, Journal of crystal growth. 112(1991) 451-457.

[16] K. L. Sweeney, L. E. Halliburton, D. A. Bryan, R.R. Rice, R. Gerson, H. E. Tomaschke, Point defects in Mg-doped lithium niobate, Journal of applied physics. 57(1985) 1036-1044.

[17] H. Qiao, J. Xu, G. Zhang, X. Zhang, Q. Sun, G. Zhang, Ultraviolet photorefractivity features in doped lithium niobate crystals, Physical Review B. **7**0 (2004) 094101.

[18] T. Volk, M. Wöhlecke, N. Rubinina, N. V. Razumovski, F. Jermann, C. Fischer, R. Böwer, $LiNbO_3$ with the damage-resistant impurity indium, Applied Physics A. 60 (1995) 217-225.

[19] Y. Kong, S. Liu, Y. Zhao, H. Liu, S. Chen, J. Xu, Highly optical damage resistant crystal: Zirconium-oxide-doped lithium niobate, Applied Physics Letters. 91(2007) 081908.

[20] G. G. Zhong, J. Jian, Z. K. Wu, In Proceedings of the Eleventh International Quantum Electronics Conference, IEEE, New York. (1980) Page 631.

[21] D. A. Bryan, R. Gerson, H. E. Tomaschke, Increased optical damage resistance in lithium niobate, Applied Physics Letters. 44(1984) 847-849.

[22] B.C. Grabmaier, F. Otto, Growth and investigation of MgO-doped $LiNbO_3$, Journal of Crystal Growth. 79(1986), 682-688.

[23] Y. Furukawa, M. Sato, F. Nitanda, K. Ito, Growth and characterization of MgO-doped $LiNbO_3$ for electro-optic devices, Journal of Crystal Growth. 99 (1990) 832-836.

[24] B. C. Grabmaier, F. Otto, Growth and investigation of MgO-doped $LiNbO_3$, Journal of Crystal Growth. 79 (1986) 682-688.

[25] N. Iyi, K. Kitamura, Y. Yajima, S. Kimura, Y. Furukawa, M. Sato, Defect structure model of MgO-doped $LiNbO_3$, Journal of solid state chemistry. 118 (1995) 148-152.

[26] J. Liu, W. Zhang, G. Zhang, Defect chemistry analysis of the defect structure in Mg-doped $LiNbO_3$ crystals, Physica status solidi (a). 156 (1996) 285-291.

[27] U. Schlarb, K. Betzler, Influence of the defect structure on the refractive indices of undoped and Mg-doped lithium niobate, Physical Review B. 50 (1994) 751-757.

[28] H. Ishizuki, I. Shoji, T. Taira, High-energy quasi-phase-matched optical parametric oscillation in a 3-mm-thick periodically poled MgO: $LiNbO_3$ device, Optics letters. 29(2004), 2527-2529.

[29] J. Zhang, Y. Chen, F. Lu, X. Chen, Flexible wavelength conversion via cascaded second order nonlinearity using broadband SHG in MgO-doped PPLN. Optics express. 16 (2008) 6957-6962.

[30] P. Sen, P. K. Sen, R. Bhatt, S. Kar, V. Shukla, K. S. Bartwal, The effect of MgO doping on optical properties of $LiNbO_3$ single crystals, Solid state communications. 129 (2004) 747-752.

[31] M. Beveridge, L. McGhee, S. G. McMeekin, M. I. Robertson, A. Ross, J. M. Winfield, Chemomechanical polishing of lithium niobate using alkaline silica sol and alkaline silica sol modified with hydrogendifluoride anion, Journal of Materials Chemistry. 4 (1994) 119-124.

[32] S. Jeong, H. Lee, H. Cho, S. Lee, H. Kim, S. Kim, J. Park, H. Jeong, Effect of additives for higher removal rate in lithium niobate chemical mechanical planarization, Applied Surface Science. 256 (2010) 1683-1688.

[33] P. Galinetto, M. Marinone, D. Grando, G. Samoggia, F. Caccavale, A. Morbiato, M. Musolino, Micro-Raman analysis on $LiNbO_3$ substrates and surfaces: Compositional homogeneity and effects of etching and polishing processes on structural properties, Optics and lasers in engineering. 45 (2007) 380-384.

[34] S. Basu, A. Zhou, M. W. Barsoum, Reversible dislocation motion under contact loading in $LiNbO_3$ single crystal, Journal of Materials Research. 23 (2008) 1334-1338.

[35] S. K. Kurtz, T. T. Perry, A powder technique for the evaluation of nonlinear optical materials, Journal of applied physics. 39 (1968) 3798-3813.

[36] D. A. Lucca, K. Herrmann, M. J. Klopfstein, Nanoindentation: Measuring methods and applications, CIRP annals- Manufacturing Technology. 59 (2010) 803-819.

[37] S. K. Jat, N. Vijayan, A. Krishna, J. Philip, S. Verma, I. Bdikin, B. Singh, G. Bhagavannarayana, S. K. Halder, Nucleation kinetics, growth, mechanical, thermal and optical characterization of sulphamic acid single crystal, CrystEngComm. 15(2013) 10034-10042.

[38] B. Riscob, R. Bhatt, N. Vijayan, I. Bhaumik, S. Ganesamoorthy, M. A. Wahab, G. Bhagavannarayana, Structural, optical and thermal properties of Zr–Fe co-doped congruent $LiNbO_3$ single crystals, Journal of Applied Crystallography. 46 (2013) 601-609.

[39] B. Riscob, I. Bhaumik, S. Ganesamoorthy, R. Bhatt, N. Vijayan, A. K. Karnal, M. A. Wahab, G. Bhagavannarayana, Effect of Mg doping on the growth aspects, crystalline perfection, and optical and thermal properties of congruent $LiNbO_3$ single crystals, Journal of Applied Crystallography. 46 (2013)1854-1862.

[40] Y. L. Chen, J. Guo, C. B. Lou, J. W. Yuan, W. L. Zhang, S. L. Chen, Z. H. Huang, G. Y. Zhang, Crystal growth and characteristics of 6.5 mol% MgO-doped LiNbO3, Journal of crystal growth. 263 (2004) 427-30

[41] S. C. Abrahams, P. Marsh, Defect structure dependence on composition in lithium niobate, Acta Crystallographica Section B: Structural Science. 42 (1986) 61-68.

[42] S. K. Kushwaha, K. K. Maurya, N. Vijayan, B. Kumar, R. Bhatt, S. Ganesamoorthy, G. Bhagavannarayana, Crystalline perfection, Raman, UV-VIS-NIR and prism coupler investigations on Cz-grown pure and Zn-doped $LiNbO_3$ single crystals, CrystEngComm. 14 (2012) 3297-305.

[43] G. Malovichko, O. Cerclier, J. Estienne, V. Grachev, E. Kokanyan, C. Boulesteix, Lattice constants of K-and Mg-doped $LiNbO_3$. Comparison with nonstoichiometric lithium niobate. Journal of Physics and Chemistry of Solids. 56 (1995) 1285-1289.

[44] B. C. Grabmaier, F. Otto, Growth and investigation of MgO-doped $LiNbO_3$, Journal of Crystal Growth. 79 (1986) 682-688

[45] F. Abdi, M. Aillerie, P. Bourson, M. D. Fontana, Defect structure in Mg-doped $LiNbO_3$: Revisited study. Journal of Applied Physics. 106 (2009) 033519.

[46] T. Ungár, Characterization of nanocrystalline materials by X-ray line profile analysis, Journal of materials science. 42(2007) 1584-1593.

[47] G. K. Williamson, W. H. Hall, X-ray line broadening from filed aluminium and wolfram, Acta metallurgica. 1 (1953) 22-31.

[48] N. V. Sidorov, M. N. Palatnikov, V. T. Gabrielyan, P. G. Chufyrev, V. T. Kalinnikov, Raman spectra and structural perfection of nominally pure lithium niobate crystals, Inorganic Materials. 43 (2007) 60-67.

[49] V. Caciuc, A. V. Postnikov, G. Borstel, Ab initio structure and zone-center phonons in $LiNbO_3$, Physical Review B. 61 (2000) 8806-8813.

[50] P. Hermet, M. Veithen, P. Ghosez, First-principles calculations of the nonlinear optical susceptibilities and Raman scattering spectra of lithium niobate, Journal of Physics: Condensed Matter. 19(2007) 456202.

[51] R. Bhatt, S. Ganesamoorthy, I. Bhaumik, A. Sexana, A. K. Karnal, P. K. Gupta, J. George, K. Ranganathan, Photorefractive properties of Fe, Zn co-doped near stoichiometric $LiNbO_3$ crystals at moderate intensities (0.5–6 W/cm^2), Optics & Laser Technology. 50 (2013)112-117.

[52] U. Schlarb, S. Klauer, M. Wesselmann, K. Betzler, M. Wöhlecke, Determination of the Li/Nb ratio in lithium niobate by means of birefringence and Raman measurements, Applied Physics A. 56 (1993) 311-315

[53] W. C. Oliver, G. M. Pharr, An improved technique for determining hardness and elastic modulus using load and displacement sensing indentation experiments, Journal of materials research. 7 (1992) 1564-1583.

[54] M. F. Doerner, W. D. Nix, A method for interpreting the data from depth-sensing indentation instruments, Journal of Materials research. 1(1986) 601-609.

[55] W. C. Oliver, G. M. Pharr, Measurement of hardness and elastic modulus by instrumented indentation: Advances in understanding and refinements to methodology. Journal of materials research. 19(2004) 03-20.

[56] S. Varughese, M. S. Kiran, U. Ramamurty, G. R. Desiraju, Nanoindentation in crystal engineering: quantifying mechanical properties of molecular crystals, Angewandte Chemie International Edition. 52 (2013) 2701-2712.

[57] S. Bhagavat, I. Kao, Nanoindentation of lithium niobate: hardness anisotropy and pop-in phenomenon. Materials Science and Engineering: A. 393(2005) 327-331.

[58] Z. Zhang, S. Yang, C. Xu, B. Wang, N. Duan, Deformation and stress at pop-in of lithium niobate induced by nanoindentation. Scripta Materialia. 77 (2014) 56-59.

[59] Fisher-Cripps, A. C. Nanoindentation, Springer, New York. 2011.

[60] M. N. Palatnikov, I . V. Biryukova, O. V. Makarova, N. V. Sidorov, O. E. Kravchenko, V. V. Efremov, Growth of large $LiNbO_3$ crystals. Inorganic Materials. 49(2013), 288-295.

Highlights

- Mg-doped lithium niobate single crystals
- Mechanical properties using nanoindentation studies
- Structural investigations by powder XRD analysis and Raman spectroscopy.

Declaration of interests

☒ The authors declare that they have no known competing financial interests or personal relationships that could have appeared to influence the work reported in this paper.

M. K. Raseel Rahman, B. Riscob, Budhendra Singh, R. Bhatt, Indranil Bhaumik, S. Ganesamoorthy, N. Vijayan, A. K. Karnal, Igor Bdikin, Lekha Nair